Corrosion and environmental sensor response delays during monitored multi-droplet wetting

Unraveling time lags in atmospheric corrosion

Vangrunderbeek, Vincent; Zhang, Keer; Coelho, Leonardo Bertolucci; Friedersdorf, Fritz; Marshall, Rebecca; Gonzalez-Garcia, Yaiza; Meeusen, Mats; Hubin, Annick; Terryn, Herman; Mamme, Mesfin Haile

DOI
10.1016/j.corsci.2025.113154

Publication date
2025

Document Version
Final published version

Published in
Corrosion Science

Corrosion Science 255 (2025) 113154

Contents lists available at ScienceDirect

Corrosion Science

journal homepage: www.elsevier.com/locate/corsci

Corrosion and environmental sensor response delays during monitored multi-droplet wetting: Unraveling time lags in atmospheric corrosion

Vincent Vangrunderbeek [a,*], Keer Zhang [b], Leonardo Bertolucci Coelho [a,c], Fritz Friedersdorf [d], Rebecca Marshall [d], Yaiza Gonzalez-Garcia [b], Mats Meeusen [a], Annick Hubin [a], Herman Terryn [a], Mesfin Haile Mamme [a]

[a] Sustainable Materials Engineering (SUME), Vrije Universiteit Brussel, Brussels, Belgium
[b] Department of Materials Science and Engineering, Faculty of Mechanical Engineering, Delft University of Technology, Delft, Netherlands
[c] IAlto Ltda, Taió, Santa Catarina, Brazil
[d] Luna Labs USA LLC, Charlottesville, VA, USA

ARTICLE INFO

Keywords:
Atmospheric corrosion sensors
Image segmentation
In-situ microscopy
Surface, relative humidity
Data-driven
Time lags

ABSTRACT

This study investigates time lags between environmental changes, electrolyte formation, and atmospheric corrosion sensor responses under controlled multi-droplet wetting. A commercial corrosion and environmental sensor was combined with in-situ microscopy, and an Artificial Intelligence (AI)-based segmentation approach was applied to track droplet growth. A cross-correlation analysis identified and quantified time lags between Surface Relative Humidity (SRH), droplet radius, and sensor responses based on Interdigitated Electrodes (IDE) measuring conductance, galvanic corrosion, and free corrosion. This approach ultimately aids in understanding how environmental fluctuations affect the dynamic behaviour of the electrolyte layer and, in turn, influence atmospheric corrosion sensor responses.

1. Introduction

Traditionally, predicting atmospheric corrosion severity involves categorizing environments based on long-term averages of environmental parameters such as Relative Humidity (RH), Temperature (T) and pollutants (sulfur dioxide and chlorides) [1]. While useful for broad assessments, this approach does not address the impact of short-term fluctuations in environmental conditions on corrosion dynamics [2]. Atmospheric corrosion sensors address this gap by capturing corrosion processes on shorter timescales [3]. However, when analysing relationships between parameters that change over time, time-dependent effects can be present [4]. These effects, often denoted as time lags, occur when changes in one variable do not immediately translate into corresponding changes in another, introducing delays in system responses [5]. Due to the cyclic nature of atmospheric corrosion, these delays can result in hysteresis and phase shifts between input and response variables. Time lags are significant since they can alter how relationships between corrosion sensor data and environmental changes are understood. This has implications for machine learning (ML) approaches, which are increasingly applied to data from atmospheric corrosion sensors to develop predictive models [6–11]. Time lag effects, if not adequately accounted for, can reduce model performance, as seen in other fields [4,5]. Despite their recognized importance in fields such as environmental sciences, time lags in atmospheric corrosion remain largely unexplored, with prior studies offering only brief acknowledgment of their possible presence [12–14]. To investigate them, it is essential to consider the electrolyte layer, which plays a central role in mediating environmental changes and atmospheric corrosion sensor responses.

To practically evaluate the electrolyte layer, the Time of Wetness (TOW) is frequently used, representing the time a metal surface is wet, a critical condition for corrosion to occur [15]. The classical understanding of TOW is an environmental variable that can be calculated through the ISO 9223 standard that classifies a surface as wet when RH $\geq$ 80 % and T > 0°C [16,17]. The concept of Surface Relative Humidity (SRH), introduced by Cole et al., more accurately describes the local moisture conditions at the surface [18]. They showed that it better represents the wet surface in comparison to traditional bulk RH. Nevertheless, a fixed (S)RH value has proven unreliable in cases where capillary condensation occurs due to corrosion product formation or

* Corresponding author.
E-mail address: vincent.vangrunderbeek@vub.be (V. Vangrunderbeek).

https://doi.org/10.1016/j.corsci.2025.113154
Received 28 February 2025; Received in revised form 30 April 2025; Accepted 29 June 2025
Available online 30 June 2025

when hygroscopic salts are present [19,20]. TOW can also be estimated as a surface parameter through indirect methods by analysing the electrolyte present on a surface exposed to atmospheric conditions. Sensors that act as surrogates for the surface of interest can be used for this purpose. These sensors are typically produced using noble metals to only measure the hygroscopic properties of deposited salts [21]. These sensors, often consisting of metal electrodes separated by insulating material, detect moisture by measuring changes in conductance when an electrolyte bridges the gap [22]. For example, Boswell-Koller et al. used conductance to categorize their corrosion dataset into dry, semi-wet and wet conditions [23]. Shinohara et al. proposed to use Atmospheric Corrosion Monitoring (ACM) sensors based on different types of galvanic couples measuring a galvanic current, to assess the TOW [24]. However, electrode-type galvanic TOW sensors that readily corrode may produce responses that are dependent on both the salt contaminants of interest and sensor metal corrosion products. In general, variations in thermal transport, emissivity, and wetting properties can influence how the electrolyte is formed [15]. Due to such differences, it remains unclear whether time lags exist between the electrolyte formation on the surface of interest and the indirect TOW sensor output, making direct observation of the electrolyte layer essential. One effective method for such observation is visual tracking, as demonstrated by Zhang et al., who employed a novel, real-time imaging method to monitor multi-droplet conditions [25]. Using an electrical resistance sensor, they were able to shed light on the relation between the droplet properties, changes in environmental parameters and the corrosion rate. Their setup simulates a mix of condensation and aerosol deposition, which are common electrolyte formation scenarios in atmospheric corrosion [15]. Condensation occurs when the air adjacent to a surface cools below the dew point, causing water vapour to condense into droplets. On the other hand, aerosol deposition results in small, dispersed droplets that settle onto the surface through impaction and gravitational settling [15, 26–30]. Since droplet formation is not driven solely by immediate changes in RH, these processes inherently involve time lags between environmental fluctuations and the appearance of droplets [31].

In this study, the established electrolyte monitoring setup of Zhang et al. was adapted to introduce a new approach for examining time lags between environmental changes, electrolyte formation and corrosion sensor responses under multi-droplet conditions [25]. Corrosion-related variables were measured using a commercially available environmental and corrosion monitoring device (Acuity LS™, Luna Labs, Charlottesville, VA, USA), combined with in-situ imaging to track the evolution of droplet radii. Experiments conducted using demineralized water and 1 M NaCl solutions captured the influence of electrolyte conductivity on the system, while a cross-correlation analysis was applied to statistically identify and quantify time lags [32,33].

2. Methodology

2.1. Experimental setup

2.1.1. Atmospheric corrosion and environmental sensor

In this study, a corrosion and environmental real-time monitoring device was utilized, illustrated in Fig. 1. This device incorporates Interdigitated Electrodes (IDE) to assess galvanic corrosion, free corrosion of individual alloys and conductance [22]. Additionally, it includes sensors for RH, Air Temperature (T_{air}) and Surface Temperature (T_{surf}) measurements. The measurement frequency of all variables was set to once per minute, which was the shortest possible interval for the device.

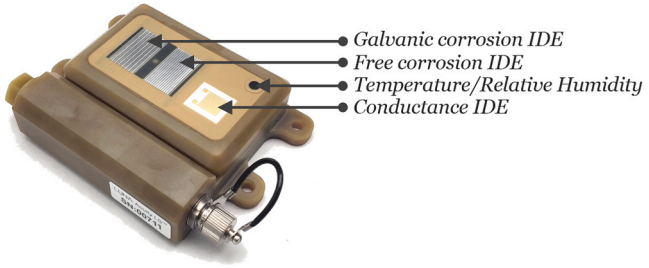

Fig. 1. The corrosion and environmental real-time monitoring device.

The free corrosion IDE is used to measure the free corrosion current using a two-electrode method where each electrode has the same area and is made from the same material. This measurement to obtain the free corrosion current is similar to that of a Linear Polarisation Resistance (LPR) technique using a low amplitude and low frequency excitation voltage. Each electrode in the sensor is fabricated from 0.8 mm thick carbon steel 1008 and designed with seven interdigitated segments of equal area, providing a total electrode area of 1.45 cm^2. The current, captured as the Root Mean Square (RMS) response to a 20 mV peak-to-peak sine wave at 0.5 Hz, spans a range from 5 nA to 100 μA and has demonstrated a strong correlation with mass loss measurements in accelerated corrosion tests [34–36]. Consequently, the measured current, obtained under a low-amplitude excitation within the linear polarization range, is assumed to be proportional to the free corrosion current under the tested conditions.

The galvanic corrosion sensor captures galvanic coupling effects and consists of two electrodes: One of aluminium alloy AA6061-T6 and the other of carbon steel 1008, separated by a 0.18 mm insulating layer. Each electrode includes seven interdigitated segments (0.8 mm wide and 25.4 mm long). Using a Zero-Resistance Ammeter (ZRA), which allows current measurement with minimal electrical resistance between the electrodes, the galvanic corrosion current is monitored between the two electrodes at equal potential. This sensor output current range is from 0.01 μA to 100 μA. Notably, the galvanic corrosion current is used here solely as an indicator of the electrolyte layer rather than a direct measure of corrosion rate.

The conductance sensor quantifies electrolyte presence and conductivity across the surface of a gold IDE. Conductance is assessed through electrochemical impedance using an excitation signal with two distinct frequencies: High-Frequency (HF) at 25 kHz and Low-Frequency (LF) at 10 Hz, both applied as a 20 mV peak-to-peak sine wave. The HF signal primarily measures solution conductance, while the LF signal is influenced by both polarization resistance and solution conductance. This dual-frequency approach extends the sensitivity to moisture and contaminants, with the HF range covering 5 μS to 10 mS and the LF range enabling detection as low as 5 nS, allowing precise assessment of low-conductivity scenarios.

The SRH has been proven to be a better metric for assessing the actual state of wetness at a surface and was calculated as follows using the environmental variables the sensor measures [37]:

$$SRH = RH \frac{P_{H_2O,sat}(T_{air})}{P_{H_2O,sat}(T_{surf})} \quad (1)$$

Where $P_{H_2O,sat}(T_{air})$ denotes the saturated vapour pressure at the ambient T, while $P_{H_2O,sat}(T_{surf})$ refers to the surface T.

The sensor was polished to Si #1200 grit to standardize surface roughness, which affects droplet formation by altering the wetting angle and corrosion initiation [38]. After polishing, the surface was cleaned with deionized water, followed by isopropanol and dried with compressed air.

2.1.2. Climate chamber and experimental conditions

A custom-designed climate chamber identical to that described by Zhang et al. was utilized to simulate multi-droplet wetting under controlled conditions [25]. This allows the measurement and analysis to focus on changes in RH, which was manipulated through the continuous introduction of very fine aerosols using an ultrasonic humidifier. Upon entering the chamber, these aerosols partially evaporate into water vapour. As such, the RH gradually increased and stabilized over time,

without active feedback or cyclical control. The T was not actively controlled and remained near room temperature, fluctuating passively in response to the aerosols/vapour mixture introduced by the humidifier. For testing, the sensor was placed horizontally in the lab-scale climate chamber. To analyse the effect of water alone, demineralized water was used initially in the humidifier to produce the aerosol/vapour mixture. This setup simulates a rural environment, allowing a focus on the impact of the electrolyte layer without interference from other contaminants. To simulate a more aggressive marine environment, a 1 M NaCl solution was introduced into the ultrasonic humidifier, generating NaCl aerosols. NaCl is widely used in experimental and mechanistic studies of droplet corrosion [30]. A high-resolution camera was utilized to capture the electrolyte evolution every minute. Both experiments were conducted for 85 min, during which the aerosol/vapour mixture was continuously forced to flow over the corrosion and environmental monitoring device. This duration allowed sufficient time for droplet stabilization and comprehensive sensor data collection. After each experiment, the chamber and humidifier were thoroughly rinsed with demineralized water to prevent cross-contamination. For complete details of the chamber components and setup, including the specifications of the camera system and lighting arrangement, refer to Zhang et al. [25].

2.2. Data analysis methods

2.2.1. Image analysis of droplet growth evolution

To measure the formation and growth of the electrolyte layer on the sensor surface, droplets were identified from images captured during both experimental conditions. Image measurements were limited to the electrolyte layer on the free corrosion sensor of the corrosion monitoring device. The open-source AI image segmentation model 'Segment Anything' (SAM) by Meta was used for droplet identification due to its ability to accurately segment objects without extensive manual annotation, making it suitable for tracking droplet growth [39]. However, defining droplet edges accurately was challenging due to variations in lighting, surface finish and the transparency of water droplets. Additionally, SAM could not inherently differentiate droplets from other surface features, such as corrosion products and polishing lines. To address these challenges, a semi-automatic labelling approach was employed. This involved manually drawing bounding boxes around droplets to guide the model in segmenting the droplets correctly. The SAM semi-automatic labelling approach was applied three times for each experimental condition to assess variability in droplet identification. The analysis focused on a zoomed-in section of the sensor surface to provide a clearer view of droplet formation, with the results assumed to represent behaviour across the entire surface. Once the droplets were identified, their areas were calculated and the average droplet radius was derived by assuming semi-spherical droplets, a common approach to represent droplet growth dynamics in similar studies [30]. An exponential smoothing function was applied to the radius data to emphasize overall growth trends while reducing noise. This analysis quantified droplet formation and growth, forming the basis for studying time-dependent effects between electrolyte layer evolution and the variables measured by the corrosion and environmental monitoring device.

2.2.2. Cross-correlation analysis

To investigate time-dependent effects in our simulated atmospheric corrosion system under controlled multi-droplet wetting, cross-correlation analysis was employed [40]. Cross-correlation is a statistical method that quantifies the correlation between two time-series variables across different time shifts, providing insight into how changes in one variable may precede changes in another [5,32,33,41]. In this study, a time lag is defined as the time shift at which the linear correlation between two variables is maximized. The variables analysed, introduced in Section 2.1.1, included SRH, droplet radius, free corrosion current, galvanic corrosion current and HF (25 kHz) and LF (10 Hz) conductance. By identifying the time lag where the correlation between variables is maximized, cross-correlation highlights the timing of their strongest linear interaction. However, while it identifies and quantifies these time lags, it does not explain their origin, which is assumed to stem from physicochemical phenomena or inherent sensor response characteristics [42].

The general steps of the cross-correlation analysis are as follows:

1. Pair cause and effect variables: Identify pairs of variables where one (the cause) is expected to influence changes in the other (the effect) based on known system relationships.
2. Compute lagged time series: Create lagged versions of the cause variable by shifting its time series forward in time across a range of time lags.
3. Calculate correlation for each lag: For each time-shifted version of the cause variable, calculate the correlation coefficient with the effect variable. This reveals how strongly changes in one variable are linearly connected to changes in the other at each time shift.
4. Identify maximum correlation and corresponding lag: Determine the time lag where the correlation coefficient reaches its maximum value. This lag represents the time delay when the two variables are most closely linked, suggesting the strongest cause-and-effect relationship.

A detailed mathematical description of cross-correlation can be found elsewhere [33]. The cross-correlation was done in a Python environment using the SciPy library.

3. Results and discussion

3.1. Droplet formation and evolution

Time-lapse images of the free corrosion sensor, taken every minute, served as the raw data for droplet evolution tracking. Droplet identification was performed using the SAM semi-automatic labelling approach, as detailed in Section 2.2.1. Fig. 2(a) illustrates the evolution of the average droplet area and the corresponding smoothed average droplet radius is shown in Fig. 2(b) for demineralized water and 1 M NaCl aerosol/vapour wetting conditions. The shaded areas represent 95 % confidence intervals, derived from three repeated applications of the SAM labelling approach per experimental condition, to account for variability in droplet identification and estimate uncertainty.

Droplet growth typically involves three key phases: Initiation, coalescence and stabilization [31]. For both experimental conditions, these stages were observed by analysing the evolution of the droplet area shown in Fig. 2(a). Initially, a slight increase in droplet area is observed, followed by a steep rise, indicating the coalescence of smaller droplets into larger ones. Finally, a flattening of the curve marks the stabilization phase. In terms of droplet radius, this is mirrored by a steady, proportional increase over time, as shown in Fig. 2(b). For both experimental conditions, the droplet radius stabilized after approximately 50 min, with droplets in the 1 M NaCl condition stabilizing at ~0.2 mm and those in the demineralized water case stabilizing at ~0.25 mm. The electrolyte layer remained in the form of discrete droplets for the complete duration of both experimental conditions.

Fig. 3 shows the SAM labelling approach to detect droplets, including raw images, bounding boxes and segmented droplets, as an example of the labelling process during droplet stabilization after 85 min. In the demineralized water condition Fig. 3(a), the model often overestimated droplet sizes due to unclear droplet boundaries. In the 1 M NaCl condition, displayed in Fig. 3(b), dark spots indicative of corrosion products are observed alongside the droplets on the steel electrodes. These made it more challenging for the model to detect edges and distinguish droplets from corroded areas.

While this study focused on droplets as a two-dimensional

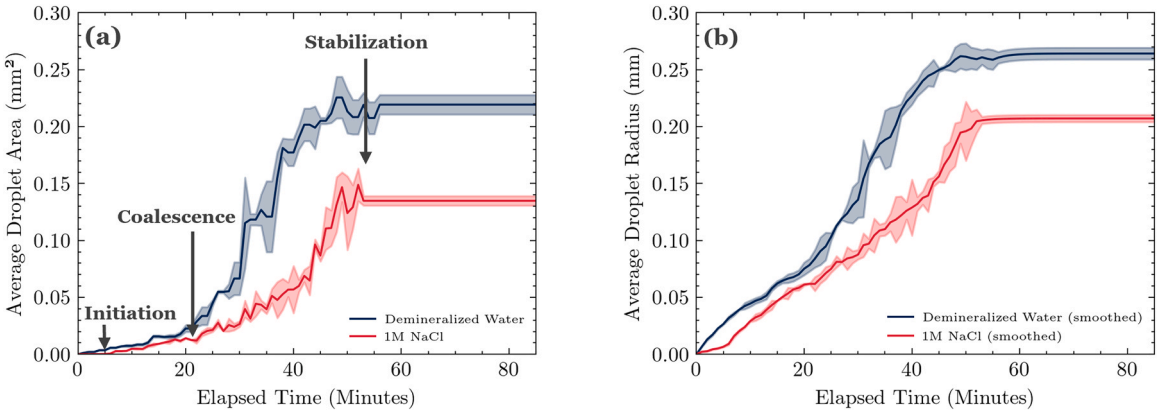

Fig. 2. (a) Average droplet area and (b) smoothed average droplet radius measured on the free corrosion sensor over time for the demineralized water and 1 M NaCl aerosol/vapour wetting experiments. Shaded regions denote the 95 % confidence interval.

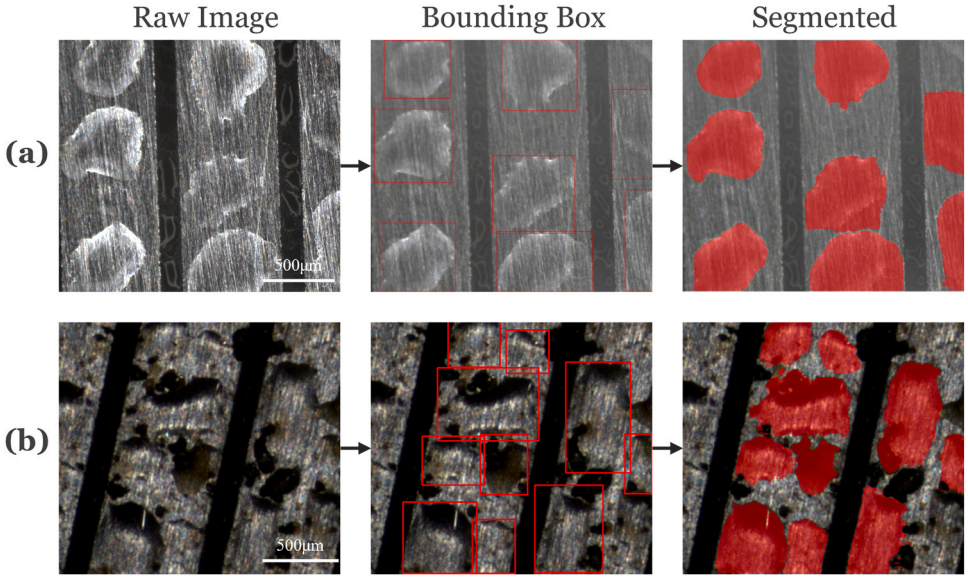

Fig. 3. Droplet segmentation for the (a) demineralized water and (b) 1 M NaCl aerosol/vapour wetting experiments using the SAM semi-automatic labelling approach. Raw images (left), bounding boxes (centre) and segmented droplets (right) illustrate the labelling process during droplet stabilization after 85 min.

observable, it is recognized that the electrolyte layer is inherently three-dimensional, and that droplet thickness can affect corrosion behaviour and, consequently, sensor responses [27,28]. Although side-view imaging can provide information on droplet height, it was not feasible for the current multi-droplet setup [27]. Zhang et al. showed that droplet edge intensity in top-view images can reflect droplet geometry, which could be explored in future studies [25].

However, given the study's aim to identify time lags within a

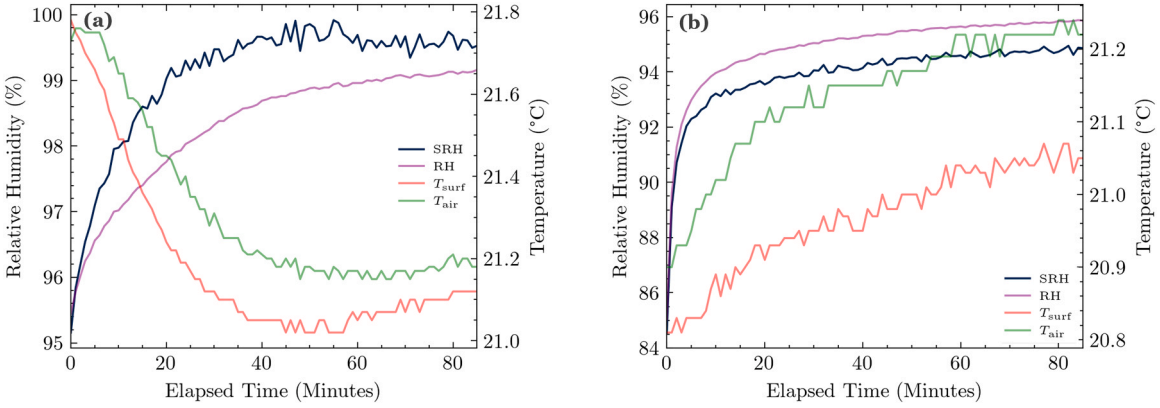

Fig. 4. (a) Demineralized water and (b) 1 M NaCl aerosol/vapour wetting experiments showing time evolution of surface temperature, air temperature, relative humidity and surface relative humidity.

relatively short experimental timeframe, the semi-automatic SAM analysis capturing two-dimensional droplet size information was sufficient to track qualitative trends in droplet evolution.

3.2. Surface relative humidity and temperature dynamics

To elucidate the conditions under which the droplets formed on the free corrosion sensor surface, the evolution of T_{surf}, T_{air}, RH and SRH (calculated via Eq. 1) was examined for both the demineralized water and 1 M NaCl condition in Fig. 4. T_{air}, which reflects the chamber temperature, was not actively controlled but allowed to fluctuate naturally. At the start of the test, T_{air} stabilized around 21.8 °C for the demineralized water condition and 20.8 °C for the 1 M NaCl condition. However, given the measurement resolution of ±0.5 °C for both T_{surf} and T_{air}, these initial temperatures are virtually the same. The RH sensor had a resolution of ±2 %. Given these errors, absolute differences should be interpreted cautiously. Nonetheless, the overall trends remain relevant for interpreting the droplet formation conditions. Fig. 4(a) shows that the RH rose from about 95–99 % during the demineralized water case. Early on, T_{surf} and T_{air} were effectively the same indicating that initial droplet formation likely stemmed from direct aerosol deposition rather than condensation which typically results from scenarios where $T_{surf} < T_{air}$ during high RH. However, throughout the rest of the testing period, $T_{surf} < T_{air}$ resulting in SRH > RH nearly reaching 100 %. This can be explained by evaporative cooling as the SRH is not saturated at 100 % but still enough aerosols are brought in to sustain droplet growth. It is likely that there is a mix between direct deposition of aerosols and condensation as the latter can occur at SRH< 100 % due to the surface orientation and flow effects [15]. For the 1 M NaCl condition displayed in Fig. 4(b), RH increased sharply before stabilizing around 96 %. The aerosols contained soluble NaCl above their deliquescence point and their exothermic hydration likely caused $T_{surf} > T_{air}$ for most of the test. Consequently, SRH < RH, stabilizing at 95 %. Ionic repulsion among dissolved salts limited droplet growth, resulting in smaller brine droplets as observed in Fig. 2(b) compared to the demineralized water case. Once droplets formed in both experimental conditions, they grew through coalescent forces and eventually stabilized.

3.3. Demineralized water aerosol/vapour mixture evolution of variables

The IDE sensor readings, including free corrosion current, galvanic current, LF conductance and HF conductance, were recorded every minute using the corrosion and environmental monitoring device throughout the demineralized water condition, which lasted 85 min. Fig. 5(a) presents the free corrosion current along with droplet radius (Section 3.1) and SRH (Section 3.2), illustrating their relationship over time, while Fig. 5(b) shows the LF and HF conductance together with the galvanic current. As shown in Fig. 5(a), the free corrosion current remains at its baseline value of 0.005 µA for the first 40 min before increasing in a consistent way with time. Fig. 5(b) highlights the galvanic current, which rises at the start and stabilizes around 0.8 µA after 65 min. Over the first 40 min, LF conductance starts with a modest

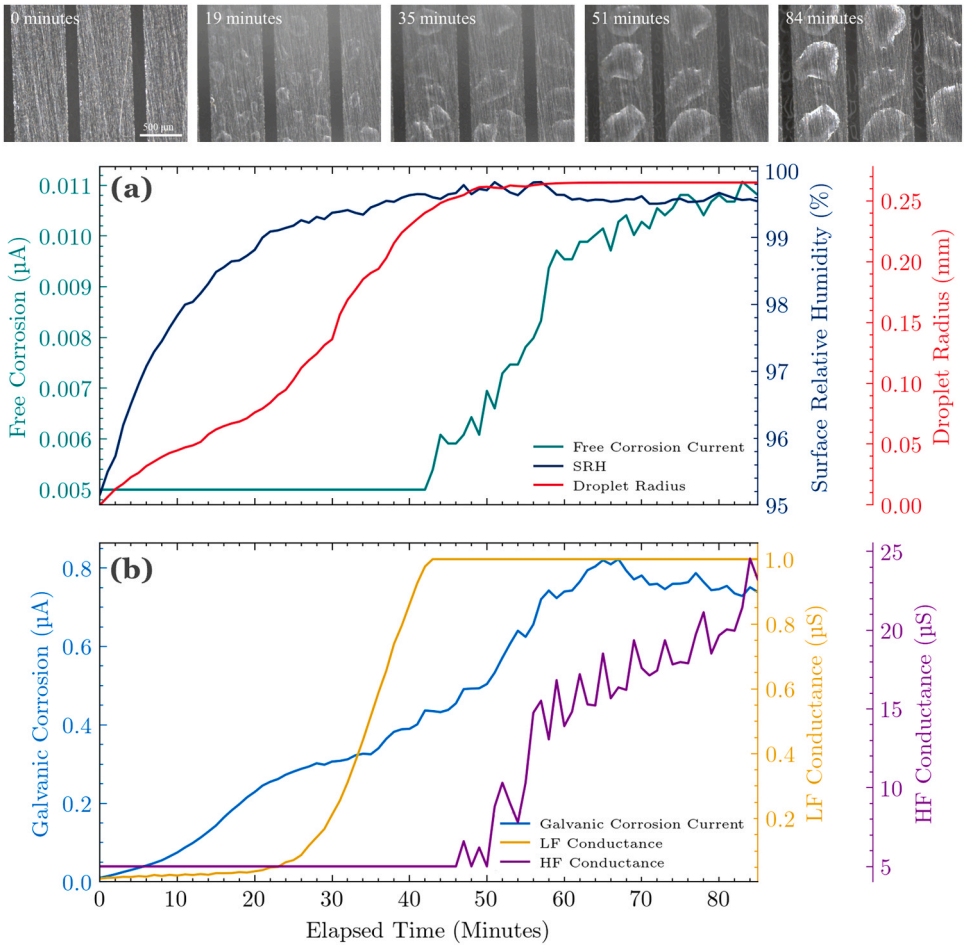

Fig. 5. Evolution of (a) droplet radius (from image analysis), surface relative humidity and free corrosion current (Fe/Fe free corrosion sensor) and (b) galvanic current (Al/Fe galvanic corrosion sensor) and conductance (EIS response of high (HF)- and low (LF)-frequency excitation signals on a gold-plated sensor) during the demineralized water aerosol/vapour wetting experiment. Surface images of the free corrosion sensor at distinct time points are shown at the top of the plots to illustrate droplet evolution.

increase that quickly accelerates, eventually leveling off at 1 μS. The HF conductance increases at 42 min and has more noise due to its broader measurement range (0.005–10 mS), which reduces sensitivity and resolution at lower conductivities compared to the narrow range (0.005–1 μS) of the LF conductance measurements.

3.3.1. M NaCl aerosol/vapour mixture evolution of variables

To investigate the effect of increased ionic content on the relationship between the droplet radius and the different variables measured by the corrosion and environmental monitoring device, a 1 M NaCl solution was used in the humidifier to generate the aerosol/vapour mixture. Fig. 6(a) shows how the free corrosion current begins increasing after 10 min, peaks near 4.5 μA at 60 min and then declines slightly. Fig. 6(b) shows that the galvanic corrosion current increases in two phases: A steep initial rise followed by a more gradual increase after 25 min, peaking at 32 μA. It then declines around the same time as the free corrosion current but at a steeper rate. The LF conductance reaches its upper limit of 1 μS almost immediately due to the high ion concentration, while HF conductance starts with a modest increase before accelerating rapidly to attain its limit of 10 mS by 44 min.

The decline in free and galvanic corrosion currents is likely due to the accumulation of corrosion products, which form a barrier that reduces oxygen diffusion and slows the corrosion rate despite the aggressive environment [43]. This interpretation is supported by observations in Fig. 3(b), which show corrosion product formation on the Fe/Fe free corrosion sensor under droplets during stabilization. Another possible explanation is that during the stabilization of the droplets, the droplet contact angle starts to increase, leading to a longer diffusion path for oxygen, thereby lowering the corrosion current [28,31]. However, as previously mentioned, droplet thickness was not measured in this study. As a result, definitive conclusions regarding the free or galvanic corrosion currents during droplet stabilization cannot be made.

3.4. Time lag determination: Cross-correlation analysis

Cross-correlation analysis was performed to analyse time lags between the system's variables, as outlined in Section 2.2.2. This method quantifies the correlation between two variables across different time lags and determines the lag at which their interaction is most significant. To illustrate the process, an example using droplet radius and free corrosion current data from the demineralized water condition is provided in Fig. 7. Although these variables were previously presented, Fig. 7(a) revisits the raw data to establish the foundation for the complete cross-correlation evaluation. In Fig. 7(b), the cross-correlation results are displayed, with the maximum correlation coefficient (0.99) and its corresponding lag (23 min) annotated. Finally, Fig. 7(c) visualizes these findings in a causal diagram, where an arrow between the variables indicates the maximum correlation and lag [44]. The direction of the arrow is chosen based on the general understanding of how the system's variables interact.

This workflow was systematically applied to all variable pairs in both experimental conditions. The resulting causal diagrams for the

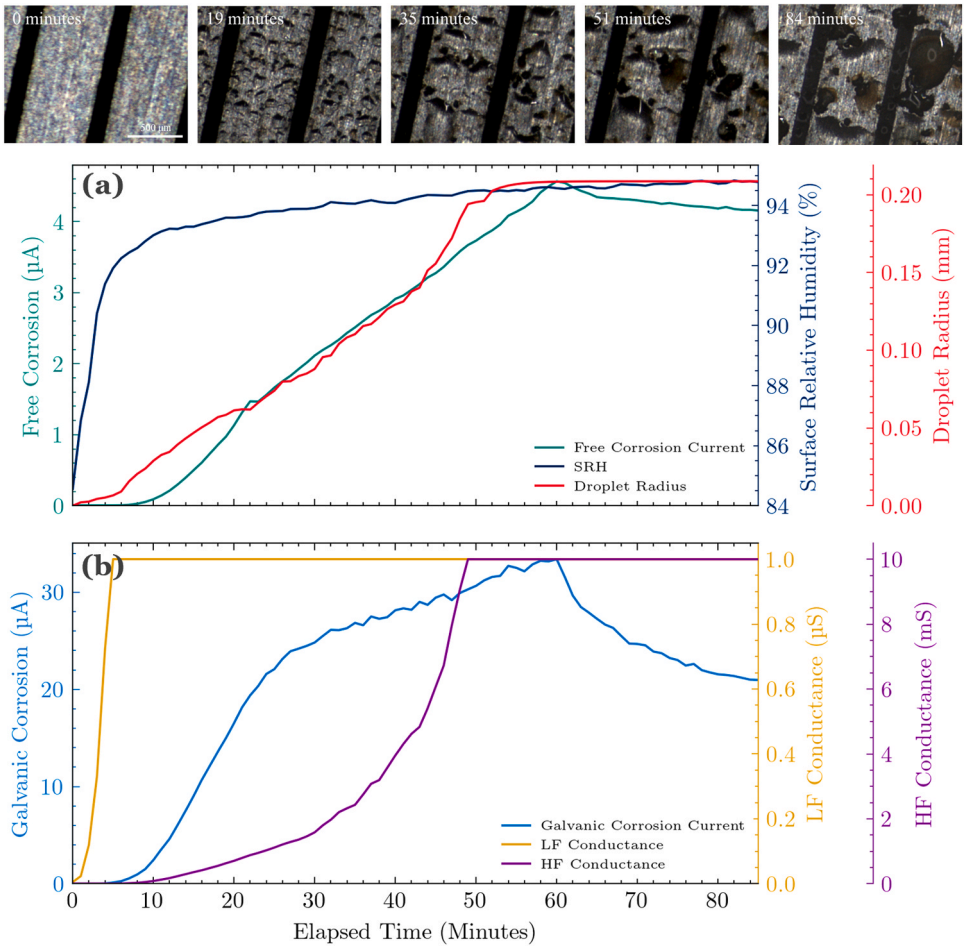

Fig. 6. Evolution of (a) droplet radius (from image analysis), surface relative humidity and free corrosion current (Fe/Fe free corrosion sensor) and (b) galvanic current (Al/Fe galvanic corrosion sensor) and conductance (EIS response of high (HF)- and low (LF)-frequency excitation signals on a gold-plated sensor) during the 1 M NaCl aerosol/vapour wetting experiment. Surface images of the free corrosion sensor at distinct time points are shown at the top of the plots to illustrate droplet evolution.

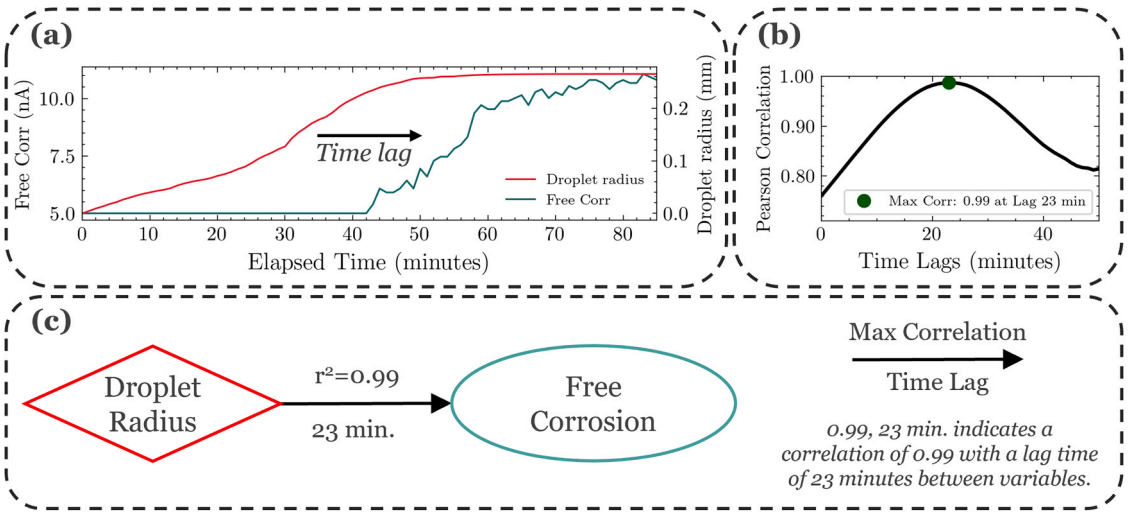

Fig. 7. Schematic illustration of the cross-correlation approach to analyse time lag relationships during the aerosol/vapour wetting experiment. (a) Temporal evolution of two system variables (droplet radius and free corrosion current shown as an example). (b) Cross-correlation plot with the maximum correlation (0.99) and corresponding lag (23 min) annotated. (c) Causal diagram depicting the relationship, with an arrow linking the two variables, annotated with the maximum correlation and lag.

demineralized water and 1 M NaCl cases are presented in Fig. 8. SRH drives droplet formation, which directly impacts HF and LF conductance measurements. These conductance changes, in turn, affect free and galvanic corrosion currents. Although 1 M NaCl alters the system's dynamics during aerosol/vapour wetting compared to demineralized water, the underlying causal relationships among environmental changes, electrolyte formation and sensor responses are assumed to remain unchanged. Detailed cross-correlation plots are available in Supplementary section A (Figure A1 for demineralized water and Figure A2 for the 1 M NaCl).

The causal diagram of the demineralized water condition shown in Fig. 8(a) indicates that the effect of SRH on droplet radius has a correlation of 0.98 at a 28-minute lag. This lag occurs because SRH stabilizes rapidly, while droplet growth proceeds more slowly through coalescence processes, remaining relatively unaffected by further variations in SRH [31]. Droplet radius influences the free corrosion current after a 23-minute lag with a correlation of 0.99. Because droplets formed by the demineralized water aerosol/vapour mixture exhibit limited ionic conductivity, fewer electrochemical reactions are expected between electrodes [26]. However, the absence of measurable free corrosion current before droplet stabilization is more likely due to insufficient electrolyte conductivity rather than a lack of actual corrosion activity. In early electrolyte stages, low solution conductance can keep free corrosion current readings below the sensor's detection limit. As atmospheric gases such as CO_2 dissolve in the droplets and form weak acids, the electrolyte conductivity gradually increases, yielding a measurable free corrosion current [45]. The Al/Fe galvanic corrosion sensor current shows a 16-minute lag relative to droplet radius, with a correlation of 0.99. This lag is initially counterintuitive because Fig. 5(b) demonstrates that the galvanic sensor responds immediately upon droplet formation, indicating superior low-end moisture sensitivity compared to the free corrosion sensor with identical geometry. Despite this immediate response, the galvanic current stabilizes later than the droplet radius. This apparent delay does not indicate a true onset lag between galvanic current and droplet formation. Instead, it reflects how cross-correlation aligns the trends of both variables over time, achieving maximum correlation when both have stabilized, even though they increase simultaneously during the initial droplet formation phase.

The HF conductance, measured by the gold IDE sensor, has a 25-minute lag and a correlation of 0.97, whereas LF conductance exhibits a minimal 2-minute lag with a correlation of 0.99. As shown in Fig. 5(b), the LF conductance responds rapidly to early droplet formation because it captures both polarization resistance and solution conductance and its range is designed for very high impedance. In contrast, the HF

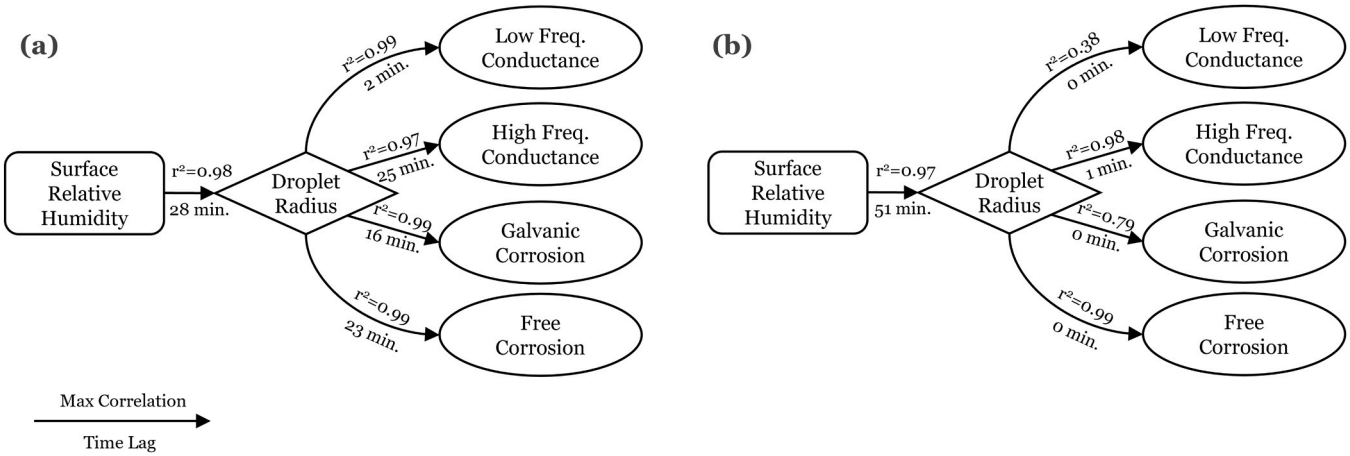

Fig. 8. Causal diagram of the (a) demineralized water and (b) 1 M NaCl aerosol/vapour wetting experiment, showing the relationships between system variables. Arrows link pairs of variables, annotated with the maximum correlation coefficient and corresponding time lag, as determined by cross-correlation analysis.

conductance primarily reflects the solution conductance at lower impedances and remains below its detection threshold until the electrolyte layer stabilizes. Consequently, in low conductance environments, LF conductance closely tracks the initial stages of droplet growth when polarization resistance dominates while HF conductance rises more gradually as the electrolyte layer becomes more conductive.

Fig. 8(b) presents the causal diagram for the 1 M NaCl condition, following the same structure discussed previously. Cross-correlation analysis between SRH and droplet radius reveals a maximum correlation of 0.97 at a 51-minute lag. This longer lag, compared to the demineralized water condition, arises from the steeper initial rise of SRH before stabilizing. The droplet radius has a correlation of 0.99 with free corrosion current at 0-minute lag, indicating a direct instantaneous relationship. The presence of Na^+ and Cl^- ions in the droplets substantially increased the contribution of solution conductance during the free corrosion current measurements compared to the demineralized water condition. Consequently, the measured free corrosion current depends primarily on the polarization resistance, allowing larger droplets to facilitate higher currents due to a larger contact area [26]. The galvanic corrosion current now exhibits 0-minute lag with respect to the droplet radius but has a lower correlation of 0.79 compared to the demineralized water condition. This decrease is attributed to the rapid decline of the galvanic current after stabilization, which reduces the linear relationship between the variables. The HF conductance follows droplet growth with a 1-minute lag and a correlation of 0.98. In contrast, the LF conductance shows no lag but has a weaker correlation of 0.38, providing limited information beyond the initial stage of droplet formation. Therefore, the HF conductance serves as a valuable indirect indicator of electrolyte evolution in highly conductive environments.

The cross-correlation approach proved effective for the purpose of this study, where the 85-minute timeframe and controlled conditions allowed reliable interpretation of time lags. However, the observed lags also reflect the specific geometry and detection principle of the free corrosion sensor, particularly the requirement for electrolyte bridging between electrodes. In longer-term studies or under more variable environmental conditions, time lags may shift and become non-linear, which should be taken into account in future time lag analysis approaches.

3.5. Comparative insights and general implications

The time lag between SRH stabilization and droplet formation is 28 min for demineralized water and 51 min for 1 M NaCl aerosol/vapour wetting condition. This delay arises from aerosol deposition and condensation, where coalescence, rather than changes in SRH, drives continued droplet growth [31]. Note that variations in salt concentration and composition can influence droplet characteristics and as such the associated time lags with respect to a changing environment [46]. Such delays suggest that TOW defined as an environmental parameter, such as the ISO 9223 definition of RH $>$ 80 % and T $>$ 0 °C as conditions capable of causing significant corrosion, may not fully capture the evolving nature of electrolyte formation. In both experimental conditions, this criterion would classify the surface as “wet” throughout the test, yet it provides no insight into how the electrolyte layer evolves, which is crucial to assess the corrosion behaviour at any given time. Therefore, similar to how environmental sciences factor in past weather to interpret current states, the observed lag between humidity stabilization and droplet formation indicates that when assessing TOW as an environmental parameter, integrating recent environmental history is expected to better capture the evolving surface wetness.

Droplet formation was directly tracked only on the free corrosion sensor and electrolyte evolution may vary across the galvanic and conductance sensors due to differences in surface properties [15]. This can lead to different electrolyte bridging patterns between the electrode digits, a necessary requirement for these IDE-based sensors to generate a signal. During the 1 M NaCl condition, Fig. 6(a) shows that the free corrosion sensor exhibited no response in the first five minutes, as the initial droplets were likely too small to bridge the electrodes. However, once bridging occurred, the signal appeared without further delay, resulting in the 0-minute lag between droplet radius and free corrosion current. This reinforces the hypothesis that the lag observed in the demineralized water condition is primarily due to low electrolyte conductivity, as previously discussed, rather than a lack of electrode bridging. In contrast, other atmospheric corrosion sensors rely on different detection principles and thus may exhibit distinct response patterns and unique time lags [3]. Conductance effectively indicated droplet formation, tracking droplet radius evolution and approximating free and galvanic corrosion onset with minimal delay. Its broad measurement range (0.005–10,000 μS), achieved by using two excitation signals at distinct frequencies, allows it to adapt to varying conductive conditions [19]. This strengthens previous work that used conductance to classify wetting stages using the corrosion and environmental monitoring device [23,47].

Unlike the conductance sensor that uses noble metal electrodes and defines "wet" conditions as the presence of a conductive electrolyte, galvanic sensors use reactive metals or alloy electrodes, where "wet" is characterized by corrosion activity, indicated by the galvanic current [15,37]. Indeed, during the demineralized water condition, the galvanic current was noisier and stabilized later than the observed droplet formation, whereas in 1 M NaCl, it exhibited two distinct increases. However, the HF conductance measurement in the 1 M NaCl case plateaued once droplets stabilized, while the galvanic sensor continued to evolve, offering a clearer indication of ongoing corrosion activity and droplet stabilization. It should be noted that the galvanic Al/Fe sensor in the corrosion and environmental monitoring device is not explicitly designed to capture electrolyte formation but instead corrosion activity. Therefore, when combined with the conductance sensor, both measurements complement each other and can be used to interpret electrolyte detection, early corrosion susceptibility and corrosion severity. Cross-correlation analysis revealed a time lag from droplet radius to galvanic current in the demineralized water case, reflecting simultaneous stabilization of both variables rather than a genuinely delayed sensor response. This result highlights the importance of domain knowledge to ensure observed time lags reflect actual physical phenomena rather than coincidental trends. While limiting the cross-correlation analysis to data collected before sensor signals reached steady-state could reduce the risk of irrelevant lags, the entire dataset was retained to highlight the necessity of informed interpretation. Fig. 9 provides a summarizing schematic overview of the methodology and key findings, highlighting the interplay between environmental changes, electrolyte formation, and sensor responses.

Although the indirect TOW sensors effectively tracked or indicated electrolyte evolution, the analysis in this study was limited to a single wetting mode and one environmental variable. In realistic outdoor exposures, additional factors such as T variations, wind speed, rain events, sunlight intensity and other weather variables could introduce their intrinsic time lags on electrolyte formation, as do diverse (de)wetting modes. Over more extended periods, the accumulation of corrosion products further influences the behaviour of the electrolyte layer. For example, previous studies have shown that corrosion products can retain moisture, prolonging wet conditions beyond what environmental variables or indirect TOW sensors with different surface properties would indicate [15]. As such, evolving surface conditions through corrosion product formation, as well as repeated salt and solid particle deposition, are expected to alter electrolyte dynamics and induce shifts in time lag behaviour during extended or cyclic exposures. The ability to continuously monitor atmospheric corrosion processes in situ is a relatively new development and these technologies open new avenues for corrosion modelling. The present study begins to address the temporal and spatial dynamics of electrolyte formation and sensor response, which are critical factors to account for in any modelling framework that aims to predict instantaneous corrosion rates as a function of time from

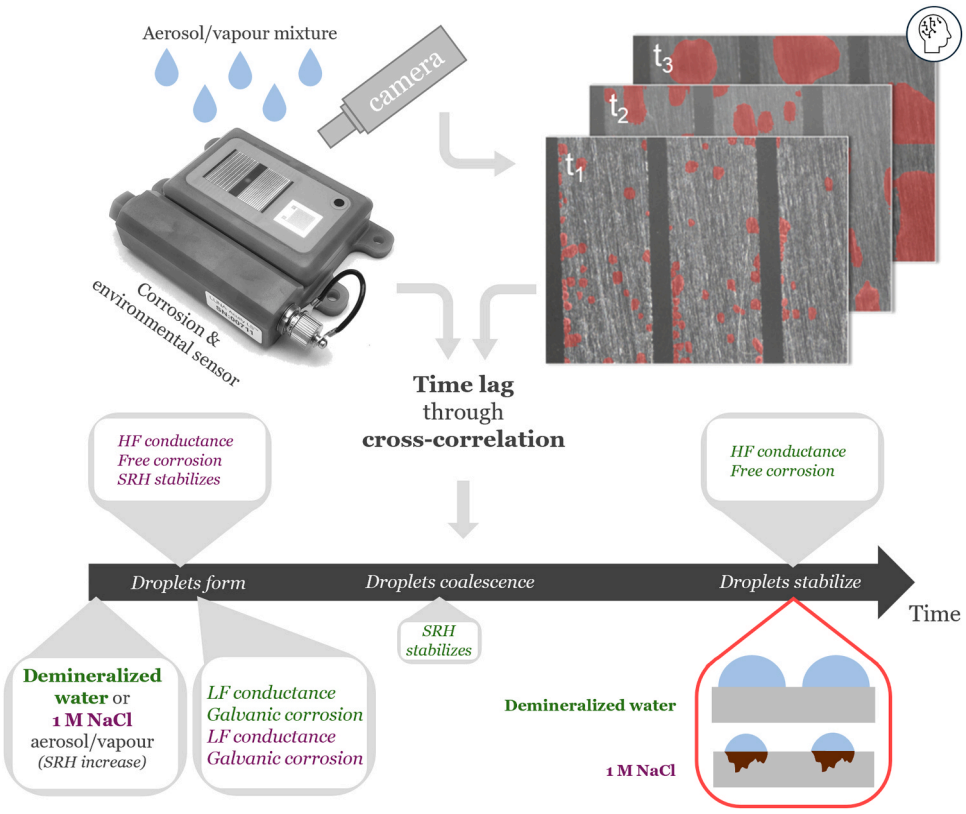

Fig. 9. Schematic overview of the study's methodology, incorporating a corrosion and environmental monitoring device, in-situ microscopy, multi-droplet wetting experiments and cross-correlation analysis, along with the key findings on electrolyte formation and sensor response time lags.

environmental conditions. Future studies should consider a broader range of environmental variables, including their cyclic nature, as well as diverse wetting modes and direct electrolyte-layer observations, such as visual monitoring, to better understand time lags in atmospheric corrosion.

4. Conclusion

A corrosion and environmental monitoring device, complemented by in-situ microscopy, was subjected to controlled multi-droplet wetting, enabling a novel way to study time lags between environmental changes, electrolyte formation and IDE-based sensor responses. The employed AI-based SAM segmentation model effectively captured droplet evolution and cross-correlation analysis quantified the resulting time lags. Results revealed that droplet formation lagged behind SRH stabilization, with 1 M NaCl conditions further extending this delay. The indirect TOW sensors (galvanic and conductance) exhibited high correlation and minimal lag with respect to droplet evolution, whereas the free corrosion sensor's response depended on electrolyte conductivity. These findings underscore the importance of direct electrolyte-layer observation for interpreting atmospheric corrosion sensor data.

https://github.com/VincentVangrunderbeek/Time-lags-atmospheric-corrosion

CRediT authorship contribution statement

Annick Hubin: Writing – review & editing, Supervision. **Herman Terryn:** Supervision. **Mesfin Haile Mamme:** Writing – review & editing, Visualization, Supervision. **Vangrunderbeek Vincent Vester:** Writing – original draft, Visualization, Methodology, Formal analysis, Data curation, Conceptualization. **Keer Zhang:** Investigation, Data curation. **Leonardo Bertolucci Coelho:** Writing – review & editing, Visualization, Methodology, Investigation. **Fritz Friedersdorf:** Writing – review & editing, Investigation. **Rebecca Marshall:** Writing – review & editing, Investigation. **Yaiza Gonzalez-Garcia:** Writing – review & editing, Resources. **Mats Meeusen:** Writing – review & editing.

Declaration of Competing Interest

The authors declare that they have no known competing financial interests or personal relationships that could have appeared to influence the work reported in this paper.

Acknowledgements

V.V. acknowledges funding from the Research Foundation – Flanders (FWO, Project 1SH5E24N). M.H.M. acknowledges funding from the Research Foundation – Flanders (FWO, project 1264221N)

Declaration of Generative AI and AI-assisted technologies in the writing process

During the preparation of this work the author(s) used ChatGPT in order to improve readability of some sentences. After using this tool/service, the author(s) reviewed and edited the content as needed and take(s) full responsibility for the content of the publication.

Appendix A. Supporting information

Supplementary data associated with this article can be found in the online version at doi:10.1016/j.corsci.2025.113154.

Data Availability

Data will be made available on request.

References

[1] A.A. Mikhailov, J. Tidblad, V. Kucera, The classification system of ISO 9223 standard and the dose–response functions assessing the corrosivity of outdoor atmospheres, Prot. Met. 40 (2004) 541–550, https://doi.org/10.1023/B:PROM.0000049517.14101.68.

[2] H. Simillion, O. Dolgikh, H. Terryn, J. Deconinck, Atmospheric corrosion modeling, Corros. Rev. 32 (3-4) (2014) 73–100, https://doi.org/10.1515/corrrev-2014-0023.

[3] K. Popova, T. Prošek, Corrosion monitoring in atmospheric conditions: a review, Metals 12 (2) (2022) 171, https://doi.org/10.3390/met12020171.

[4] J.De Stefani, Towards Multivariate Multi-Step-Ahead Time Series Forecasting: A Machine-Learning Perspective, Université libre de Bruxelles, 2022.

[5] A.P. Nicolau, K. Dyson, D. Saah, N. Clinton, in: J.A. Cardille, et al. (Eds.), Exploring lagged effects in time series, Cloud-Based Remote Sensing with Google Earth Engine, Springer, 2024, pp. 403–420, https://doi.org/10.1007/978-3-031-26588-4_21.

[6] V. Vangrunderbeek, et al., Exploring the potential of transfer learning in extrapolating accelerated corrosion test data for long-term atmospheric corrosion forecasting, Corros. Sci. 225 (2023) 111619, https://doi.org/10.1016/j.corsci.2023.111619.

[7] Z. Pei, et al., Towards understanding and prediction of atmospheric corrosion of an Fe/Cu corrosion sensor via machine learning, Corros. Sci. 170 (2020) 108697, https://doi.org/10.1016/j.corsci.2020.108697.

[8] Y. Cai, Y. Xu, Y. Zhao, X. Ma, Atmospheric corrosion prediction: a review, Corros. Rev. 38 (4) (2020) 299–321, https://doi.org/10.1515/corrrev-2019-0100.

[9] L.B. Coelho, et al., Reviewing machine learning of corrosion prediction in a data-oriented perspective, npj Mater. Degrad. 6 (1) (2022) 8, https://doi.org/10.1038/s41529-022-00218-4.

[10] A. Venkatraman, et al., An active learning framework for the rapid assessment of galvanic corrosion, npj Mater. Degrad. 8 (1) (2024) 54, https://doi.org/10.1038/s41529-024-00476-4.

[11] R.S. Marshall, et al., Galvanic corrosion between coated Al alloy plate and stainless-steel fasteners, Part 2: application of finite element method and machine learning to study galvanic current distributions, Corrosion 79 (2) (2023) 157–173, https://doi.org/10.5006/4153.

[12] J. Runge, et al., Inferring causation from time series in Earth system sciences, Nat. Commun. 10 (2019) 2553, https://doi.org/10.1038/s41467-019-10105-3.

[13] J.F. Stanners, Use of environmental data in atmospheric corrosion studies, Br. Corros. J. 5 (1970) 117–121, https://doi.org/10.1179/000705970798324748.

[14] B. Daneshian, D. Höche, O.Ø. Knudsen, A.W.B. Skilbred, Effect of climatic parameters on marine atmospheric corrosion: correlation analysis of on-site sensors data, npj Mater. Degrad. 7 (1) (2023) 10, https://doi.org/10.1038/s41529-023-00329-6.

[15] E. Schindelholz, R.G. Kelly, Wetting phenomena and time of wetness in atmospheric corrosion: A review, Corros. Rev. 30 (2012), https://doi.org/10.1515/corrrev-2012-0015.

[16] EN ISO 9223: 2012. Corrosion of Metals and Alloys, Corrosivity of Atmospheres, Classification, Determination and Estimation, 2021.

[17] D. Camuffo, A. della Valle, F. Becherini, A critical analysis of one standard and five methods to monitor surface wetness and time-of-wetness, Theor. Appl. Climatol. 132 (2018) 1143–1151, https://doi.org/10.1007/s00704-017-2167-9.

[18] I.S. Cole, et al., A study of the wetting of metal surfaces in order to understand the processes controlling atmospheric corrosion, J. Electrochem. Soc. 151 (12) (2004) B627, https://doi.org/10.1149/1.1809596.

[19] P. Norberg, Surface moisture and time of wetness measurements, 2002.

[20] E. Schindelholz, B.E. Risteen, R.G. Kelly, Effect of relative humidity on corrosion of steel under sea salt aerosol proxies: II. $MgCl_2$, artificial seawater, J. Electrochem. Soc. 161 (2014) C460, https://doi.org/10.1149/2.0231410jes.

[21] E. Schindelholz, Towards Understanding Surface Wetness and Corrosion Response of Mild Steel in Marine Atmospheres, Ph.D. thesis, Univ. of Virginia, 2014.

[22] ISO 22858:2020. Corrosion of metals and alloys — Electrochemical measurements — Test method for monitoring atmospheric corrosion, 2020.

[23] C.N. Boswell-Koller, V. Rodriguez-Santiago, Statistical analysis of environmental parameters: correlations between time of wetness and corrosion severity, Corrosion 75 (5) (2019) 498–504, https://doi.org/10.5006/2970.

[24] D. To, T. Shinohara, O. Umezawa, Experimental investigation on the corrosivity of atmosphere through the atmospheric corrosion monitoring (ACM) sensors, ECS Trans. 75 (29) (2017) 1, https://doi.org/10.1149/07529.0001ecst.

[25] K. Zhang, et al., Monitoring atmospheric corrosion under multi-droplet conditions by electrical resistance sensor measurement, Corros. Sci. 236 (2024) 112271, https://doi.org/10.1016/j.corsci.2024.112271.

[26] T.H. Muster, et al., The atmospheric corrosion of zinc: The effects of salt concentration, droplet size and droplet shape, Electrochim. Acta 56 (2011) 1866–1873, https://doi.org/10.1016/j.electacta.2010.09.099.

[27] E. Rahimi, et al., Atmospheric corrosion of iron under a single droplet: a new systematic multi-electrochemical approach, Corros. Sci. 235 (2024) 112171, https://doi.org/10.1016/j.corsci.2024.112171.

[28] N. Van den Steen, et al., Predicting the effect of droplet geometry and size distribution on atmospheric corrosion, Corros. Sci. 202 (2022) 110308, https://doi.org/10.1016/j.corsci.2022.110308.

[29] H.A. Terryn, et al., Comparing modelling and experiments for prediction of atmospheric corrosion under controlled dynamic thin-film and droplet electrolytes, ECS Meet. Abstr. 242 (2022), https://doi.org/10.1149/MA2022-0211712mtgabs.

[30] B.G. Koushik, et al., Review on modelling of corrosion under droplet electrolyte for predicting atmospheric corrosion rate, J. Mater. Sci. Technol. 62 (2021) 254–267, https://doi.org/10.1016/j.jmst.2020.04.061.

[31] J.E. Castillo, J.A. Weibel, S.V. Garimella, The effect of relative humidity on dropwise condensation dynamics, Int. J. Heat. Mass Transf. 80 (2015) 759–766, https://doi.org/10.1016/j.ijheatmasstransfer.2014.09.080.

[32] W.N. Probst, V. Stelzenmüller, H.O. Fock, Using cross-correlations to assess the relationship between time-lagged pressure and state indicators, ICES J. Mar. Sci. 69 (2012) 670–681, https://doi.org/10.1093/icesjms/fss015.

[33] P. Bourke, "Cross correlation," Cross-Correlation, Auto-Correlation – 2D Pattern Identification, 1996.

[34] S. Kopitzke, A. Lilly, K. Canales, Characterizing environmental severity for Naval Air Stations, DoD. Corros. Conf. (2023).

[35] R. Marshall, V. Avance, L. Askew, F. Friedersdorf, Environmental severity classification of atmospheric corrosion using electrochemical monitoring, Mater. Perform. Charact. (2024).

[36] L. Agnew, R. Marshall, V. Avance, C. Brandi, F. Friedersdorf, Environmental severity classification development for aerospace-relevant materials, Mater. Perform. (2024).

[37] M. Hoseinpoor, T. Prošek, L. Babusiaux, J. Mallégol, Toward more realistic time of wetness measurement by means of surface relative humidity, Corros. Sci. 177 (2020) 108999, https://doi.org/10.1016/j.corsci.2020.108999.

[38] H.U. Sajid, R. Kiran, Influence of corrosion and surface roughness on wettability of ASTM A36 steels, J. Constr. Steel Res. 144 (2018) 310–326, https://doi.org/10.1016/j.jcsr.2018.01.023.

[39] A. Kirillov, et al., Segment Anything. in Proc, IEEE/CVF ICCV, 2023, pp. 4015–4026.

[40] T. De Kerf, et al., Identification of corrosion minerals using short-wave-infrared hyperspectral imaging, Sensors 22 (2022) 407, https://doi.org/10.3390/s22010407.

[41] U. Seeboonruang, An application of time-lag regression technique for assessment of groundwater fluctuations in a regulated river basin: a case study in Northeastern Thailand, Environ. Earth Sci. 73 (2015) 6511–6523, https://doi.org/10.1007/s12665-014-3872-7.

[42] R.S. Marshall, et al., Leveraging physical and virtual on-aircraft sensors to inform maintenance practices, AMPP CORROSION, 2024.

[43] D. de la Fuente, I. Díaz, J. Simancas, B. Chico, M. Morcillo, Long-term atmospheric corrosion of mild steel, Corros. Sci. 53 (2) (2011) 604–617, https://doi.org/10.1016/j.corsci.2010.10.007.

[44] J. Pearl, Theoretical impediments to machine learning with seven sparks from the causal revolution, arXiv preprint arXiv:1801.04016, 2018.

[45] C. Leygraf, I.O. Wallinder, J. Tidblad, T. Graedel, Atmospheric Corrosion, Wiley, 2016, https://doi.org/10.1002/9781118762134.

[46] C.R. Bryan, et al., Physical and chemical properties of sea-salt deliquescent brines as a function of temperature and relative humidity, Sci. Total Environ. 824 (2022) 154462, https://doi.org/10.1016/j.scitotenv.2022.154462.

[47] A. Lilly, S. Kopitzke, I. Long, Development of corrosion severity assessment algorithms using environmental monitoring sensors in Naval aviation environments, AMPP CORROSION, 2024.